Gels

International Edition: DOI: 10.1002/anie.201508641
German Edition: DOI: 10.1002/ange.201508641

Linking Semiconductor Nanocrystals into Gel Networks through All-Inorganic Bridges

Amita Singh, Beth A. Lindquist, Gary K. Ong, Ryan B. Jadrich, Ajay Singh, Heonjoo Ha, Christopher J. Ellison, Thomas M. Truskett, and Delia J. Milliron**

Abstract: *For colloidal semiconductor nanocrystals (NCs), replacement of insulating organic capping ligands with chemically diverse inorganic clusters enables the development of functional solids in which adjacent NCs are strongly coupled. Yet controlled assembly methods are lacking to direct the arrangement of charged, inorganic cluster-capped NCs into open networks. Herein, we introduce coordination bonds between the clusters capping the NCs thus linking the NCs into highly open gel networks. As linking cations (Pt^{2+}) are added to dilute (under 1 vol %) chalcogenidometallate-capped CdSe NC dispersions, the NCs first form clusters, then gels with viscoelastic properties. The phase behavior of the gels for variable [Pt^{2+}] suggests they may represent nanoscale analogues of bridged particle gels, which have been observed to form in certain polymer colloidal suspensions.*

All-inorganic nanocrystal (NC) solids can be synthesized by replacing native organic capping ligands with inorganic ligands, such as chalcogenidometallate clusters (ChaMs, also called MCCs)[1] and this modular approach has successfully been applied to fabricate transistors[1a] and thermoelectric devices.[1b,2] In these materials, the integrity of semiconductor NCs can be maintained as discrete building blocks and the embedded heterointerfaces are essential in determining properties. On the other hand, methods for assembling organic-ligand capped NCs are remarkably advanced such that, in addition to dense solids, porous structures ranging from honeycomb lattices[3] to gel networks[4] can be synthesized. The very low density and high internal surface area of NC gels, in particular, makes them intriguing materials for sensing, catalysis, and separations.[5]

We sought to develop a chemical method for assembling ChaM-capped NCs into gel networks by using the ChaMs as anchors for coordinating metal ions that act as linkers, joining adjacent NCs in the network. Most semiconductor NC gels have been synthesized by kinetically arrested flocculation induced by the oxidative degradation of organic capping ligands, especially thiols.[4a,6] However, Eychmüller and coworkers have demonstrated that NCs capped with tetrazolate ligands can be made to form very low density wet gels (about 1 vol % solid, based on their reported mass concentration of 70 mg mL^{-1}) by linking one NC to the next via coordination bonds between the ligands and added Cd^{2+} or Zn^{2+} ions.[4b,7] This linking method inspired our approach by which modular inorganic gel compositions—selecting independently the NCs and ChaMs—can conceivably be customized to create diverse functional inorganic networks.

To make inorganic-linker-mediated NC gels, we first exchanged the native oleate ligands on CdSe NCs with ChaMs to form a charge-stabilized dispersion in the polar solvent formamide. The ChaM $[Ge_2Se_6]^{4-}$, synthesized as a hydrazinium salt[8] was chosen as a prototype, though gel formation was also observed when using the sulfide analogue, $[Ge_2S_6]^{4-}$, the synthesis of which was also previously reported,[1c] and using antimony (Sb^{3+}) linker ions (Figure S1 in the Supporting Information). The ligand exchange proceeded by phase transfer of the NCs from toluene to a ChaM solution in formamide, then the ChaM-capped NCs were washed and dispersed again in formamide. The size and morphology of the NCs (observed by transmission electron microscopy (TEM, Figure 1 a)) was unaffected by the ligand exchange process and they retained their characteristic excitonic absorption features (Figure 1 b). Fourier transform infrared (FTIR) spectroscopy reveals that the organic ligands are removed (Figure 1 c). To evaluate the adsorption of the ChaM, we characterized the ligand-exchanged NCs by Raman spectroscopy. Although the most dominant vibrational mode of the clusters overlaps with the strong longitudinal-optical (LO) phonon mode of CdSe, the weaker peaks that arise from stretching of terminal Ge–Se bonds are resolvable (Figure 1 d). Comparing to the spectrum of the isolated ChaM (Figure S2), these peaks are shifted to higher frequency by 10–15 cm^{-1}, consistent with ChaM adsorption to the CdSe surface. As a result of surface functionalization by these anionic clusters, the zeta potential of the NCs becomes strongly negative following ligand exchange (Figure 1 e). Based on elemental analysis by inductively coupled plasma-optical emission spectroscopy and the size of the NCs observed by TEM, there are 56 ChaMs on average per NC and the aerial surface density of ChaMs is 0.88 nm^{-2}.

Gelation of the ChaM-functionalized CdSe NCs could be induced by adding potassium tetrachloroplatinate (K_2PtCl_4) to a 0.36 vol % NC dispersion in formamide. Our choice of K_2PtCl_4 was inspired by the gelled coordination networks reported by Kanatzidis, et al. when that reagent was com-

[*] Dr. A. Singh, Dr. B. A. Lindquist, G. K. Ong, Dr. R. B. Jadrich, Dr. A. Singh, H. Ha, Prof. C. J. Ellison, Prof. T. M. Truskett, Prof. D. J. Milliron
McKetta Department of Chemical Engineering
University of Texas at Austin
Austin, Texas, 78712 (USA)
E-mail: truskett@che.utexas.edu
milliron@che.utexas.edu
G. K. Ong
Department of Materials Science and Engineering, University of California Berkeley, Berkeley, California 94720 (USA)

Supporting information for this article is available on the WWW under http://dx.doi.org/10.1002/anie.201508641.

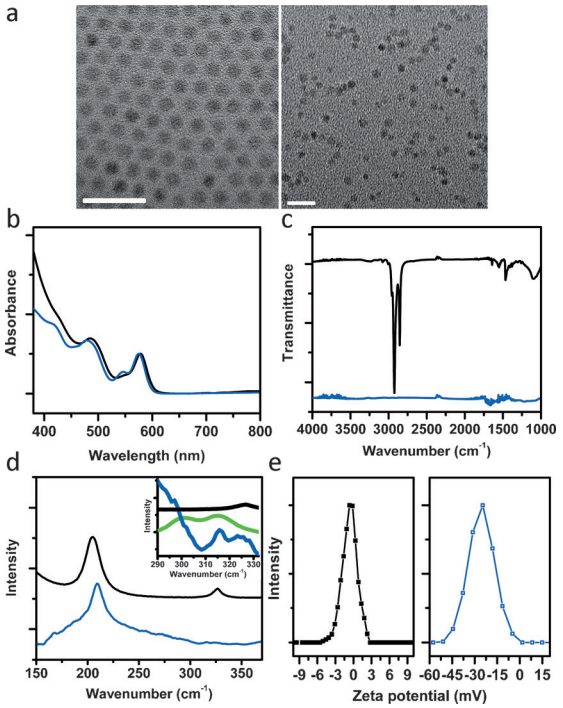

Figure 1. a) TEM b) UV/Vis absorption c) FTIR d) Raman and e) Zeta potential of CdSe NCs before (black lines, TEM left) and after ligand exchange (blue lines, TEM right) with $[Ge_2Se_6]^{4-}$. The inset to (d) is a magnified comparison of the Raman spectra of CdSe NCs before ligand exchange (black), $[Ge_2Se_6]^{4-}$ (green) and NCs after ligand exchange (blue). The scale bars in (a) are 20 nm.

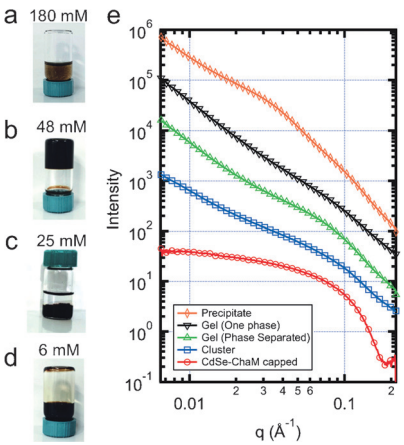

Figure 2. a–d) Photographs of ChaM-functionalized CdSe NC dispersions following the equilibration with increasing concentrations of K_2PtCl_4 from bottom to top. e) The scattering patterns of a CdSe–ChaM NC dispersion (red), of NC clusters (blue), a phase-separated gel (green), a single-phase gel (black), and a precipitated (orange) NC dispersion found at progressively higher K_2PtCl_4 concentration. The data have been vertically offset for clarity. For both the photographs and SAXS samples, the concentration of K_2PtCl_4 was 6 mM, 25 mM, 48 mM, and 180 mM (from bottom to top).

bined with anionic clusters related to our ChaMs, such as $[Ge_4Se_{10}]^{4-}$.[9] The CdSe–ChaMs dispersions darkened significantly over about 2 h after adding K_2PtCl_4. A similar dark coloration was observed in the absence of CdSe NCs, suggesting that a Pt–ChaM coordination complex forms in both cases.[9] Below a critical concentration of the K_2PtCl_4 linker (around 7.5 mM), the NC dispersion remained fluid (Figure 2d); however, at higher concentrations of $[K_2PtCl_4]$, an indefinitely stable gel formed after 16 to 24 h. Above 7.5 mM and under 48 mM of $[K_2PtCl_4]$, the system equilibrates to a phase-separated gel and clear fluid (Figure 2c). At 48 mM of $[K_2PtCl_4]$, the second critical linker concentration, a single-phase gel is formed (Figure 2b). To confirm the role of K_2PtCl_4 in gel formation and determine if gelation might result from non-specific screening of the surface charge, we replaced K_2PtCl_4 with KCl. Even at 50 mM KCl the CdSe–ChaM dispersion remained fluid, reinforcing our expectation that coordination bonds between the ChaMs and Pt^{2+} complex are responsible for gelation. Furthermore, no gel formed in the absence of NCs for similar ChaM and Pt^{2+} concentrations. Ultimately, at K_2PtCl_4 concentrations above 180 mM the NCs visibly aggregated and, over time, precipitated (Figure 2a). The Pt^{2+} linker oxidation state and Se oxidation states in the CdSe–ChaM gel was confirmed using X-ray photoelectron spectroscopy (XPS; Figure S3). Furthermore, the persistence of the CdSe NCs was verified by X-ray diffraction (XRD; Figure S4).

We monitored the assembly process by small angle X-ray scattering (SAXS, Figure 2e), which is well suited to analyzing nanoscale structure of gels.[10] In the absence of the Pt^{2+} linker, scattering of a CdSe–ChaMs dispersion reflects the form factor of monodisperse, isolated NCs with 24 Å radius. Upon addition of the linker, even below the threshold for gelation, a significant increase in scattering is observed at lower q. To interpret the SAXS data, scattering patterns were analyzed with a unified fit approach utilizing multiple levels of Guinier and Porod regime fits to account for each apparent characteristic length scale of structure (see Supporting Information, Figure S5–S8 and Table S1).[11] At the lowest linker concentrations, two characteristic length scales were apparent, one with characteristic radius of gyration, R_g of 19.06 Å, gives rise to a broad peak at $q = 0.09$ Å^{-1}, which is ascribed to scattering by the NCs. (NCs with a radius of 24 Å would have an expected R_g of 18.6 Å.) At low $q < 0.015$ Å^{-1}, the sloping scattering profile can be fit by a Porod component, with an exponent of 1.68, which—considering the observation of a free flowing fluid—can be interpreted as clustering of the NCs.[12] At higher linker concentrations that give rise to either two-phase or single-phase gels, the slope at low q changes noticeably, giving rise to a Porod exponent around 2.4, characteristic of a three-dimensional fractal structure, which are expected to have Porod exponents between 2 and 3.[13] This characteristic scattering feature is attributed to the formation of a percolated gel network as the CdSe–ChaMs building blocks are bridged by Pt^{2+} linkers.

At the highest linker concentrations, a broad peak at intermediate q around 0.03 Å^{-1} appears, which yields a characteristic R_g of 58 Å and Porod exponent between 3.1–3.5. The higher Porod exponent suggests a globular precipitate structure, rather than a mass fractal. However, the low q signature of the space-filling fractal is also present. Hence, it is likely that the structure at this high K_2PtCl_4 concentration consist of a mixture of globular precipitates and mass fractal

structure, both constructed from CdSe–ChaMs building blocks. Cumulatively, the SAXS data suggest that K_2PtCl_4 linkers induce clustering of the NCs at low concentration, induce precipitation at higher concentration, but facilitate the formation of a percolated gel network composed of NCs at intermediate concentrations.

The inorganic bridges link CdSe NCs into a network with characteristic viscoelastic properties despite the extremely low solid content (< 1 vol% based on a mass concentration of 25 mg mL^{-1}) of the wet gel. Gels are characterized by a solid-like elastic response under oscillatory frequency sweep (Figure 3) and strain sweep (Figure S9), such that the elastic

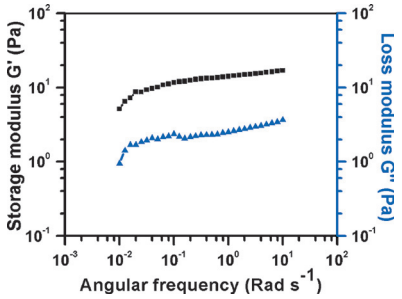

Figure 3. Frequency-dependent elastic storage modulus G' (black) and viscous loss modulus G'' (blue) of a NC linker gel with linker concentration $[Pt^{2+}] = 48$ mM, corresponding to a single-phase gel.

modulus (G') is expected to significantly exceed the viscous modulus (G'').[5b,14] The moduli were measured at 2% strain, within the linear response regime based on variable strain measurements (Figure S9). The storage modulus (G') of our single-phase NC gels is on the order of 10 Pa and is always significantly larger than the loss modulus (G'') in the range of 0.01 and 10 rads^{-1}. This indicates that the gel is behaving as a viscoelastic solid gel, considerably softer than conventional polymer melts but stronger than a typical suspension of colloids. Together with the moderate frequency dependence of the moduli, these observations are characteristic of a rheologically weak gel whose structure can likely be rearranged to some extent on the time scale of the measurement.[15] We expect the rheology of these materials could be tailored over a broad range by changes, such as varying linker concentrations or modulating strength of linker interactions, and this will be the subject of future investigations. Xerogels of inorganic linker gels were obtained by replacing the formamide with de-ionized water and then freeze-drying. A surface area of 173.52 m^2 g^{-1} was determined by Brunauer–Emmett–Teller (BET) analysis (Figure S10). The surface area of the xerogel is higher than the value reported by Brock and co-workers for a CdSe NC gel prepared by surface oxidation using tetranitromethane and bench-top drying.[4a,16] The microporosity of the xerogel is consistent with collapse of more open meso- or macro-pores during the drying process, which is apparent also by scanning electron microscopy (Figure S11).

The progression of the phase behavior with increasing linker concentration, from fluid to phase-separated gel to single-phase gel, can be understood using a theoretical framework recently employed by Liu and co-workers to elucidate the nature of gelation in a polystyrene colloidal suspension (1.8 μm colloidal particles) mediated by a polyacrylamide linker.[17] Their theoretical calculations, which model the system as a binary hard sphere mixture where unlike particles are mutually attracted, predict the equilibrium phase behavior as a function of the linker-to-particle ratio. Only in the presence of an intermediate linker concentration does a spinodal boundary emerge on the phase diagram, which predicts the formation of two phases (Figure S12). The need for intermediate linker concentration can be understood as follows: at low concentrations not enough bridging bonds form to achieve percolation and only clusters are formed, while at higher concentrations, the particle surfaces become nearly saturated with adsorbed linker, which also limits the number of bridging bonds that can be formed.

The good agreement found between the experimental conditions for gelation and the calculated spinodal boundaries in the polymer colloid study[17] strongly suggests that the underlying driving force for gelation of such linker-mediated gels is thermodynamic in nature. Though, for the polymer colloids, two-phase behavior was not observed, as slowing dynamics arrested the system in a single-phase, non-equilibrium gel. By contrast, our NC gels obtain complete phase separation between a higher density gel phase and a mostly clear fluid phase (Figure 2c). In fact, although not discussed, similar two-phase behavior was shown in photographs of organic ligand-metal cation linked NC gels reported previously.[4b] Our NC-based linker gels may therefore be more suitable than polymer colloids to experimentally realize the rich phase behavior suggested by the theory. Moreover, the realization of a single-phase gel at higher K_2PtCl_4 concentrations is a particularly exciting avenue for future research. The model suggests that gel densities can be tuned by varying linker-to-particle ratio and that gelation can be thermoreversible for moderate interaction strength. By varying the selection of ChaMs and linking cations, we expect our NC gels can demonstrate such interesting responsive behaviors. Considering the possibility of achieving rich, dynamic phase behavior and the diverse inorganic chemistries accessible, these ChaM-mediated linker gels represent an exciting new direction for functional NC-based materials.

Experimental Section

CdSe NCs with average size of 4.3 ± 0.3 nm (from TEM), with first excitonic peak at ca. 575 nm were synthesized using a published procedure.[18] Briefly, a 200 mM solution of cadmium-oleate in octadecene was heated to 120 °C and degassed for 30 min under nitrogen atmosphere. The solution was then heated to 270 °C and after it became optically clear, it was cooled to 120 °C and degassed again for 30 min. At this temperature, 0.5 M oleylamine was injected and heated to 270 °C. 1.0 M TOP-Se was injected and the reaction mixture was continued for 20 min. After the reaction, the NCs were washed with (1:2) toluene:isopropanol and redispersed in toluene.

ChaMs were prepared in a nitrogen glovebox by dissolving metal chalcogenides in anhydrous hydrazine in the presence of excess chalcogen at room temperature. The Ge–Se ChaM was synthesized by mixing 1.0 mmol of $GeSe_2$ and 1.0 mmol of Se in 1.0 mL of anhydrous hydrazine and stirring for a week. The optically clear yellow solution was filtered through a 0.2 μm filter to remove any undissolved solids

and then dried under nitrogen flow to obtain a yellow powder with the chemical formula $(N_2H_5)_4Ge_2Se_6$. Ge-S ChaM was synthesized similar to Ge-Se ChaM (1.0 mmol of GeS and 2.0 mmol of S in 1.0 mL of anhydrous hydrazine and stirred for two weeks). For ligand exchange, the ChaM ligand was dissolved in formamide at a concentration approximately 15 mg mL^{-1}. ***Caution!*** *Hydrazine is highly toxic and should be handled with extreme caution to prevent exposure by inhalation or absorption through the skin.*

Single-phase gels were prepared in a nitrogen glovebox by adding 96 mM potassium tetrachloroplatinate in formamide to CdSe–ChaMs NC solution in equal volumes, thus reducing the K_2PtCl_4 concentration by half. The two solutions were mixed well and left undisturbed for gelation. Adding 12, 50, and 360 mM of K_2PtCl_4 linker, give the clusters, two-phase gel, and precipitated samples, respectively. The NC volume fractions were calculated from the mass of NCs used and using the bulk density of CdSe = 5.82 g cm^{-3}.

The transmission electron microscope (TEM) images were obtained using a JEOL 2010F instrument. The samples were drop-casted on ultrathin carbon TEM support films (Ted Pella).

The absorption spectra of CdSe and ChaMs-capped NC were acquired on a Cary series UV/Vis-NIR spectrophotometer (Agilent) with toluene and formamide as blank solvents, respectively. The spectra were background subtracted.

The FTIR spectra were recorded on a VERTEX 70 (Bruker). The CdSe and ChaMs-capped NC were drop-casted on calcium fluoride (CaF_2) windows and spectra were taken in transmission. The data was background subtracted using a blank CaF_2 window.

Raman measurements of CdSe, ChaMs-capped CdSe NCs, and $[Ge_2Se_6]^{4-}$ ChaMs were carried at room temperature on a Horiba Jobin Yvon LabRAM ARAMIS system. The solution spectra of all the samples were obtained using a 1 cm path length quartz cuvette. A green laser (wavelength = 532 nm) was used for excitation.

The surface charge of the samples was measured using Zetasizer Nano ZS (Malvern Instruments) with a dip-cell setup.

SAXS was carried out at the Lawrence Berkeley National Laboratory Advance Light Source beamline 7.3.3 at 3.6 m sample-detector distance. Calibration was done using a silver behenate standard.[19] Ligand capped NC dispersions were in toluene while ChaM capped NCs and gel samples were in formamide enclosed in glass capillaries (Charles-Supper Company, Boron Rich, 1.5 mm diameter, 0.01 mm wall thickness) in transmission geometry. Control samples containing neat solvent were used for background subtraction. Data extraction and fitting was performed using the Nika and Irena tool suite for modeling and analysis of SAXS data.[11b,20] Specifically, circular averaging was used to convert the 2D detector data into 1D data for analysis and interpretation. The Modeling II module was used to fit NC form factors while the Unified Fit tool was used to fit the data for R_g, P, and other accompanying parameters.

Elemental analysis of CdSe and ChaMs-capped NCs was carried out using inductively coupled plasma atomic emission spectroscopy (Varian 710-ES). The NC samples were digested overnight in concentrated HNO_3 and then diluted (10 mL) to make a 2% nitric acid solution (by volume). The Cd:Se ratio was calculated as 1.16:1. The number of surface ChaMs was calculated from the ratio of Cd atoms and Ge atoms. The surface density of ChaMs was calculated from the surface area of 4.5 nm NCs and ratio of Cd:Ge = 1:0.14.

The X-ray photoelectron spectroscopy (XPS) measurements were carried out on Kratos X-ray Photoelectron Spectrometer—Axis Ultra DLD system equipped with an aluminium X-ray source. The spectrometer was equipped with a series of chambers and a capsule, known collectively as ROX interface, which allow for air-free transfer from a glove box. XPS spectra were calibrated to the C1s peak at 284.6 eV. High-resolution spectra of the Pt 4f peaks were acquired and analysis was done using the CasaXPS software package.

The rheological experiment was conducted on a shear rheometer (TA Instruments, AR-2000EX) using a 25 mm parallel upper plate with a gap of 1000 μm and a Peltier lower plate fixture for temperature control. First, strain sweep and time sweep experiments were conducted to identify the linear viscoelastic regime and to ensure the stability of the measured values over time. The frequency sweep was conducted from 0.01 rad s^{-1} to 10 rad s^{-1} at 25 °C with 2% strain.

To form a xerogel, the gel underwent solvent exchange from formamide to de-ionized water and was then freeze-dried by immersing into liquid nitrogen for 2 min then pulling vacuum at room temperature for 2 days. The nitrogen adsorption/desorption isotherm of the xerogel was measured using a surface analyzer (Quantachrome, NOVA 2200E) to obtain properties, such as BET specific surface area and pore size distribution by BJH method. Before measurements, the xerogel was degassed under vacuum at 120 °C overnight. Specific surface area was calculated by BET equation in the relative pressure range from 0.2 to 0.4 with an accuracy of $R^2 > 0.999$.

The powder X-ray diffraction of powdered gel sample was obtained using the Rigaku MiniFlex 600 instrument. For SEM imaging Zeiss Supra 40 V Scanning Electron Microscope (SEM) was used. The sample was deposited on the Si substrate and grounded using copper contacts.

Acknowledgements

SAXS data were collected on beamline 7.3.3 at the Advanced Light Source at the Lawrence Berkeley National Laboratory, a user facility supported by the Office of Science, Office of Basic Energy Sciences, of the U.S Department of Energy (DOE) under contract no. DE-AC02-05CH11231. G.K.O was supported by a National Science Foundation Graduate Research Fellowship under grant number DGE 1106400. Aj.S. was supported by the Bay Area Photovoltaics Consortium, sponsored by DOE EERE and Am.S. by a DOE Early Career grant to D.J.M., D.J.M., and T.M.T. acknowledge support of the Welch Foundation (F-1848 and F-1696, respectively). We acknowledge Dr. Hugo Celio for his help with the XPS analysis.

Keywords: bridging ligands · colloids · gels · phase behavior · semiconductor nanocrystals

How to cite: *Angew. Chem. Int. Ed.* **2015**, *54*, 14840–14844
Angew. Chem. **2015**, *127*, 15053–15057

[1] a) M. V. Kovalenko, M. Scheele, D. V. Talapin, *Science* **2009**, *324*, 1417–1420; b) Y. Ma, M. Liu, A. Jaber, R. Y. Wang, *J. Mater. Chem. A* **2015**, *3*, 13483–13491; c) R. Tangirala, J. L. Baker, A. P. Alivisatos, D. J. Milliron, *Angew. Chem. Int. Ed.* **2010**, *49*, 2878–2882; *Angew. Chem.* **2010**, *122*, 2940–2944.

[2] Y. Zhang, M. L. Snedaker, C. S. Birkel, S. Mubeen, X. Ji, Y. Shi, D. Liu, X. Liu, M. Moskovits, G. D. Stucky, *Nano Lett.* **2012**, *12*, 1075–1080.

[3] C. Stowell, B. A. Korgel, *Nano Lett.* **2001**, *1*, 595–600.

[4] a) J. L. Mohanan, I. U. Arachchige, S. L. Brock, *Science* **2005**, *307*, 397–400; b) V. Lesnyak, S. V. Voitekhovich, P. N. Gaponik, N. Gaponik, A. Eychmüller, *ACS Nano* **2010**, *4*, 4090–4096.

[5] a) N. Gaponik, A.-K. Herrmann, A. Eychmüller, *J. Phys. Chem. Lett.* **2012**, *3*, 8–17; b) S. Bag, M. G. Kanatzidis, *J. Am. Chem. Soc.* **2010**, *132*, 14951–14959.

[6] a) L. Korala, S. L. Brock, *J. Phys. Chem. C* **2012**, *116*, 17110–17117; b) I. U. Arachchige, S. L. Brock, *Acc. Chem. Res.* **2007**, *40*, 801–809; c) X. Gao, R. J. Esteves, T. T. H. Luong, R. Jaini, I. U. Arachchige, *J. Am. Chem. Soc.* **2014**, *136*, 7993–8002; d) A.

Hitihami-Mudiyanselage, K. Senevirathne, S. L. Brock, *ACS Nano* **2013**, *7*, 1163 – 1170.
[7] a) D. Wen, A.-K. Herrmann, L. Borchardt, F. Simon, W. Liu, S. Kaskel, A. Eychmüller, *J. Am. Chem. Soc.* **2014**, *136*, 2727 – 2730; b) V. Lesnyak, A. Wolf, A. Dubavik, L. Borchardt, S. V. Voitekhovich, N. Gaponik, S. Kaskel, A. Eychmüller, *J. Am. Chem. Soc.* **2011**, *133*, 13413 – 13420; c) C. Rengers, S. V. Voitekhovich, S. Kittler, A. Wolf, M. Adam, N. Gaponik, S. Kaskel, A. Eychmüller, *Nanoscale* **2015**, *7*, 12713 – 12721.
[8] D. B. Mitzi, *Inorg. Chem.* **2005**, *44*, 3755 – 3761.
[9] S. Bag, P. N. Trikalitis, P. J. Chupas, G. S. Armatas, M. G. Kanatzidis, *Science* **2007**, *317*, 490 – 493.
[10] a) D. W. Schaefer, J. E. Martin, *Phys. Rev. Lett.* **1984**, *52*, 2371; b) M. Djabourov, A. H. Clark, D. W. Rowlands, S. B. Ross-Murphy, *Macromolecules* **1989**, *22*, 180 – 188.
[11] a) G. Beaucage, H. K. Kammler, S. E. Pratsinis, *J. Appl. Crystallogr.* **2004**, *37*, 523 – 535; b) J. Ilavsky, P. R. Jemian, *J. Appl. Crystallogr.* **2009**, *42*, 347 – 353.
[12] a) B. Hammouda, D. L. Ho, S. Kline, *Macromolecules* **2004**, *37*, 6932 – 6937; b) B. Hammouda, *Polymer* **2009**, *50*, 5293 – 5297.
[13] a) H. D. Bale, P. W. Schmidt, *Phys. Rev. Lett.* **1984**, *53*, 596; b) D. W. Schaefer, K. D. Keefer, *Phys. Rev. Lett.* **1986**, *56*, 2199.
[14] C. W. Macosko, *Rheology: Principles, Measurements, and Applications*, Wiley-VCH, New York, **1994**.
[15] S. Ikeda, K. Nishinari, *J. Agric. Food Chem.* **2001**, *49*, 4436 – 4441.
[16] I. U. Arachchige, J. L. Mohanan, S. L. Brock, *Chem. Mater.* **2005**, *17*, 6644 – 6650.
[17] a) J. Luo, G. Yuan, C. Zhao, C. C. Han, J. Chend, Y. Liu, *Soft Matter* **2015**, *11*, 2494 – 2503; b) J. Chen, S. R. Kline, Y. Liu, *J. Chem. Phys.* **2015**, *142*, 084904.
[18] E. M. Chan, C. Xu, A. W. Mao, G. Han, J. S. Owen, B. E. Cohen, D. J. Milliron, *Nano Lett.* **2010**, *10*, 1874 – 1885.
[19] A. Hexemer, W. Bras, J. Glossinger, E. Schaible, E. Gann, R. Kirian, A. MacDowell, M. Church, B. Rude, H. Padmore, *J. Phys. Conf. Ser.* **2010**, *247*, 012007.
[20] a) F. Zhang, J. Ilavsky, G. G. Long, J. P. G. Quintana, A. J. Allen, P. Jemian, *Metall. Mater. Trans. A* **2010**, *41*, 1151 – 1158; b) A. Nelson, *Appl. Crystallogr.* **2006**, *39*, 273 – 276; c) G. Beaucage, *J. Appl. Crystallogr.* **1995**, *28*, 717 – 728; d) J. Ilavsky, *J. Appl. Crystallogr.* **2012**, *45*, 324 – 328.

Received: September 15, 2015
Published online: October 16, 2015

